remote sensing

MDPI

Article

A CNN-Based Method of Vehicle Detection from Aerial Images Using Hard Example Mining

Yohei Koga *, Hiroyuki Miyazaki and Ryosuke Shibasaki

Center for Spatial Information Science (CSIS), University of Tokyo, 5-1-5 Kashiwanoha, Kashiwa-shi, Chiba 2778568, Japan; heromiya@csis.u-tokyo.ac.jp (H.M.); shiba@csis.u-tokyo.ac.jp (R.S.)

* Correspondence: y.koga@csis.u-tokyo.ac.jp; Tel.: +81-4-7136-4290

Received: 31 October 2017; Accepted: 16 January 2018; Published: 18 January 2018

Abstract: Recently, deep learning techniques have had a practical role in vehicle detection. While much effort has been spent on applying deep learning to vehicle detection, the effective use of training data has not been thoroughly studied, although it has great potential for improving training results, especially in cases where the training data are sparse. In this paper, we proposed using hard example mining (HEM) in the training process of a convolutional neural network (CNN) for vehicle detection in aerial images. We applied HEM to stochastic gradient descent (SGD) to choose the most informative training data by calculating the loss values in each batch and employing the examples with the largest losses. We picked 100 out of both 500 and 1000 examples for training in one iteration, and we tested different ratios of positive to negative examples in the training data to evaluate how the balance of positive and negative examples would affect the performance. In any case, our method always outperformed the plain SGD. The experimental results for images from New York showed improved performance over a CNN trained in plain SGD where the F1 score of our method was 0.02 higher.

Keywords: vehicle detection; hard example mining; high-resolution; aerial image; satellite image; convolutional neural network (CNN)

1. Introduction

Recently, vehicle detection methods have achieved very high performance owing to deep learning techniques; moreover, many more sources of high-resolution aerial and satellite images have become available and affordable. Worldview3 by Digital Globe [1] provides images with a resolution of 0.3 m per pixel, and now many startup companies such as Planet Labs [2] and Black Sky [3] plan to launch small satellites and provide images with a resolution typically around one meter per pixel. For aerial images, in Japan, NTT Geospace [4] provides aerial images that cover 83% of Japan and updates them frequently. In this context, vehicle detection is now being applied to practical issues such as traffic volume surveys and the estimation of economic activity on the ground.

Research and development of object detection techniques have significantly progressed in recent years by the advancement of deep learning techniques, in particular, the convolutional neural network (CNN). Region-based CNN (R-CNN) [5] was one of the earliest algorithms to employ CNN for object detection and to demonstrate its great capability. In R-CNN, image regions that possibly contain target objects (called "region proposals") are chosen by a selective search algorithm [6], and then a CNN algorithm is applied to map target objects in the region proposals. Following R-CNN, many descendants have been proposed. Fast R-CNN [7] and the Spatial Pyramid Pooling network (SPP-net) [8] have improved accuracy and runtime over R-CNN by utilizing an RoI pooling layer—a special case of the spatial pyramid pooling (SPP) layer—and a SPP layer, respectively. They compute a feature map from an entire image only once, and by utilizing the RoI pooling layer or SPP layer,

they classify region proposals by projecting each of them onto that feature map, whereas R-CNN classifies each region proposal independently. However, they also employ a selective search to search region proposals in a target image, which can be time consuming. In Faster R-CNN [9], the selective search is replaced with region proposal networks (RPN). In Faster R-CNN, RPN calculates region proposals from an input image and Fast R-CNN network classifies the region proposals, while these two networks share the same feature map. Faster R-CNN is comprised of only deep learning networks and is 900% faster than Fast R-CNN. However, Faster R-CNN still has room to improve by directly connecting the RPNs and the classifier network. You Look Only Once (YOLO) [10] and Single Shot Multibox Detector (SSD) [11] include such methods, where both the region proposal function and the classification function are embedded in a single network. In these methods, possible object locations (bounding boxes) and class confidences are simultaneously predicted at each pixel of a feature map. These two methods are much faster than Faster R-CNN, while achieving almost the same or even higher accuracy.

CNN-based object detection methods, including the ones described above, have been applied to vehicle detection. Chen et al. [12] classified sliding windows, which are bounding boxes densely scattered over an entire image, by a CNN that was enhanced by ramifying the last block of convolutional and pooling layers into three different branches to deal with different scales. They achieved much higher accuracy than those using conventional methods by combining the histogram of oriented gradients (HOG) [13] feature descriptor and the support vector machine (SVM) classifier. Qu et al. [14] employed the Binarized Normed Gradients (BING) [15] algorithm, where gradient features are learnt and used for detecting possible object locations, to obtain region proposals and significantly improved the runtime over [12], while keeping the same level of accuracy as [12]. Faster R-CNN has difficulty when directly applied to vehicle detection in satellite and aerial images, because such images are much larger than natural images and target vehicles are much smaller than objects in natural images. Tang et al. [16] solved this by using enhanced RPNs that utilize a shallow fine feature map and by splitting large target images into small tiles, which are recombined after detection. Similarly, in [17], large images were split into small tiles and fed into YOLO [10] for vehicle detection. While methods such as Faster R-CNN and YOLO are becoming prevalent, the sliding window and region proposal methods are still useful, as they are easy to implement and can adopt any kind of network architecture as a classifier, for instance, a very deep network or novel network architecture. Mundhenk et al. [18] proposed a large open vehicle detection dataset called the "Cars Overhead with Context (COWC)" dataset, and evaluated the usability of context information for vehicle detection. They adopted the sliding window method with a rich model based on GoogLeNet [19] and ResNet [20], which achieved high accuracy on their COWC dataset.

While we have shown that vehicle detection methods have improved greatly, the effective use of training data has not been well studied even given its great potential to improve training results, especially in cases where training data are sparse. In practice, data are often sparse in our region of interest and obtaining additional data is usually costly. If we need to train a classifier using only such sparse data, the obtained classifier would be unable to discriminate detailed features. Therefore, it is important to extract as much useful information as possible from the training data. As an alternative, it is also possible to use a classifier trained in a different place where data are abundant. However, the training data acquired from other regions do not necessarily yield better accuracy than the one acquired from the original region. We can improve accuracy by fine-tuning such classifiers with data from our region of interest, but the effective use of training data is also important in these cases.

Nevertheless, to our knowledge, this topic does not seem to have been sufficiently studied. Tang et al. [16] employed hard example mining (HEM)—a method to weight more informative samples in learning processes to improve accuracy—by replacing the final classifier part of their Faster R-CNN-based model with a cascade of boosted classifiers of shallow decision trees. In each stage of their Real AdaBoost [21] training, one of the candidate weak classifiers, which best classified the training data, was selected as a part of the final classifier. The misclassified examples were weighted,

and the candidate weak classifiers in the next stage were imposed on well classifying those weighted hard examples. While their attempt succeeded, they did not focus on improving the feature learning part in terms of the effective use of training data, which is more straightforward.

In this paper, we proposed the application of HEM to the feature learning process of a CNN model for vehicle detection from high-resolution aerial images.

2. Methodology

We applied HEM to the stochastic gradient descent (SGD), a commonly used algorithm in deep learning training. Specifically, we used a large batch size, and in each batch, calculated the loss values and employed only examples with the largest loss values for training. In this way, we could always use the most informative examples for training and to improve accuracy.

The details are as follows. In Section 2.1, we introduce our basic methodology and its drawbacks. We first introduce our vehicle detection steps and then explain the characteristics of SGD where there is room for improvement. In Section 2.2, we briefly introduce the related studies of HEM and explain the details of our method. In Section 2.3, we explain our method of accuracy assessment for the experiments in this paper.

2.1. Basic Methodology

In this paper, we used a simple sliding window method for vehicle detection. Candidate bounding boxes were scattered densely over an entire image and then those with no existence of vehicles were screened out. HEM was applied to the training of CNN used for the screening. Employed CNN architecture was also simple. We employed the simple sliding window method and CNN architecture, because we mainly focused on the effectiveness of our HEM method. Our HEM method is easily scaled, for instance, by replacing the CNN architecture with a richer one, such as the model used in [18].

Our HEM method was actually a variant of Online Hard Example Mining (OHEM) [22], which was originally designed for Fast R-CNN, but required modifications to suit our method as our training process and the Fast R-CNN training process were different. (The details are described in Section 2.2.)

2.1.1. Vehicle Detection Methodology

We structured the algorithm based on the method of [12]. Figure 1 shows our CNN architecture.

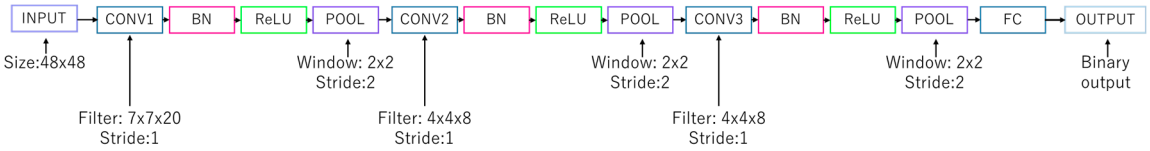

Figure 1. The CNN architecture employed in this study. We introduced batch normalization layers to accelerate learning.

CONV, BN, ReLU, POOL, FC represent the convolutional layer, batch normalization layer, Rectified Linear Unit layer, and fully connected layer, respectively. While we simplified the CNN architecture of [12], we added batch normalization [23] layers to accelerate the learning process.

The window size was set so that it finally became 50 pixels before classification, which was large enough to cover a typical vehicle size (see details of our data in Section 3.1). The detailed vehicle detection steps are as follows:

- Threshold a test image by pixel intensity greater than 60 or less than 100 and calculate gradient images, yielding three gradient images (Figure 2).
- Generate sliding windows that overlap each other on half of width and height (Figure 3).

- Move centers of the windows to geometric centers, which represent possible positions of objects in windows. Geometric centers are calculated as Equation (1):

$$\boldsymbol{g}_{\text{center}} = \sum_{i}^{W}\sum_{j}^{H} \frac{\boldsymbol{p}_{i,j} I_{i,j}}{S}$$
$$S = \sum_{i}^{W}\sum_{j}^{H} I_{i,j} \tag{1}$$

  where $\boldsymbol{g}_{\text{center}}$ is a vector which express a pixel position of a geometric center; W and H are the width and height of a window patch, respectively (both are equal to the window size); vector $\boldsymbol{p}_{i,j}$ is a pixel position $(i,\ j)$ $(1 \leq i \leq W,\ 1 \leq j \leq H)$; $I_{i,j}$ is a gradient intensity value of a pixel $(i,\ j)$; and S is the sum of the gradient intensity values at all pixels in a window patch (Figure 4a,b).
- Enlarge them by a factor of $\sqrt{2}$, and move them to the new geometric centers (Figure 4c,d).
- Discard unnecessary windows that were close to the others. We regarded the windows whose centers were within a distance of 0.15 of window size as unnecessary (Figure 5).
- Apply a CNN to RGB pixels in the windows remaining after the above steps.
- Examine if the windows had overlapping windows with more than 0.5 of IoU from the highest probability of vehicle existence to the lowest. If a window had overlapping windows, the overlapping windows were discarded (this is called non-maximum-suppression).

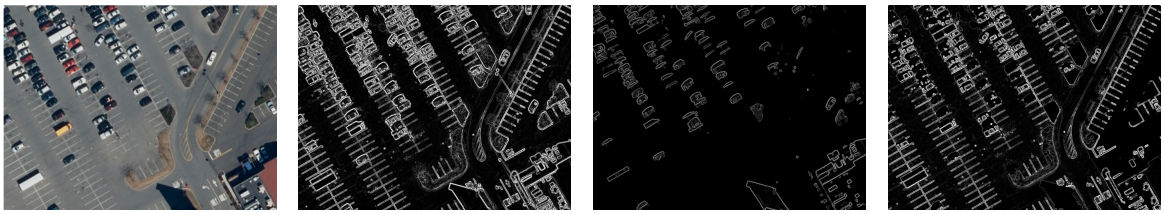

(**a**) (**b**) (**c**) (**d**)

Figure 2. Original image and calculated gradient images. (**a**) Original image; (**b**) gradient of the original image; (**c**) gradient of the image thresholded over 60; (**d**) gradient of the image thresholded under 100.

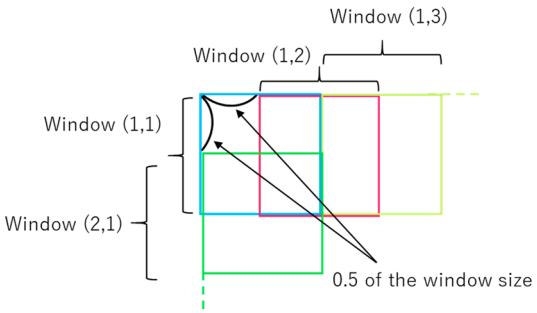

Figure 3. How sliding windows are spaced in an image.

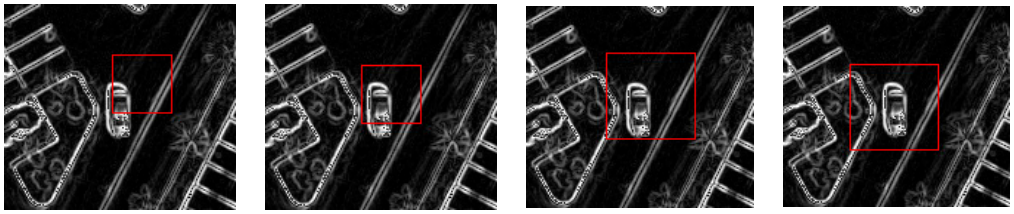

Figure 4. An example of a sliding window move. (**a**) An initial window; (**b**) moved to its geometric center; (**c**) enlarged; (**d**) moved to its new geometric center.

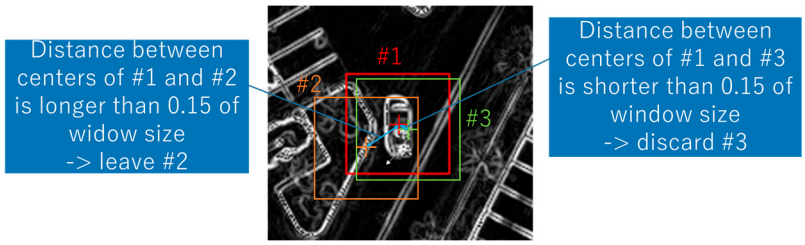

Figure 5. How to discard unnecessary windows.

We did not use any meta information such as shadow directions. In terms of sliding window accuracy, we evaluated the negative impact of clutter and shadows in the Appendix A.

2.1.2. Stochastic Gradient Descent (SGD) and Room for Improvement

SGD is an algorithm for optimizing parameters in machine learning that is commonly used in deep learning. First, we explain gradient descent (also called batch gradient descent) on which SGD is based. In machine learning, parameters are optimized by minimizing the objective function (also often called the loss function). In gradient descent, a parameter is updated by

$$\theta \leftarrow \theta - \alpha \nabla_{\theta} J(\theta) \tag{2}$$

where θ is the parameter, α is the learning rate, J is the objective function, and its derivative $\nabla_{\theta} J(\theta)$ is called the gradient. In gradient descent, gradients are calculated over all examples in the training data and used to update θ [24,25]. This is repeated until there is convergence. However, this becomes inefficient or infeasible when the number of training data is huge [24,25]. Hence in SGD, a small number of examples—called a minibatch—are sampled from the entire training dataset and used for training. Sampling a minibatch is random as giving training data in some meaningful order can bias gradients and lead to poor convergence [25]. Specifically, all of the training data are first shuffled [25] and partitioned (usually equally) into minibatches, then each minibatch is processed for optimization in order. Strictly speaking, this should be called minibatch gradient descent, and SGD originally meant using only a single training example [24]; however, we use this term as it is commonly used in a deep learning context. This is based on the assumption that each minibatch approximates the entire training dataset well [24]. One minibatch process is called an iteration, and processing the entire dataset is called an epoch. Training continues over epochs until convergence.

Now let the weight variables of our model be $\boldsymbol{W}$, minibatch input data be $\boldsymbol{X}$, labels (the numbers which express the classes) of $\boldsymbol{X}$ be $\boldsymbol{T}$, and loss function be $L(\boldsymbol{W}, \boldsymbol{X}, \boldsymbol{T})$. Note that if x and t are single examples of $\boldsymbol{X}$ and $\boldsymbol{T}$, respectively, $L(\boldsymbol{W}, \boldsymbol{X}, \boldsymbol{T})$ must be the summation of all $L(\boldsymbol{W}, x, \mathrm{t})$ [26]. Given

concrete input $\boldsymbol{X}$ and labels $\boldsymbol{T}$, we can regard the $\boldsymbol{X}$ and $\boldsymbol{T}$ as the coefficients of L. Therefore, L is regarded as a function of $\boldsymbol{W}$. We can interpret Equation (2) as follows:

$$\mathbf{W} \leftarrow \mathbf{W} - \alpha \nabla_{\mathbf{W}} L(\mathbf{W}, \mathbf{X}, \mathbf{T}) \tag{3}$$

This equation updates $\boldsymbol{W}$ so that the loss function becomes smaller. As a consequence, the model becomes able to classify input well. The gradient of each weight variable is calculated by propagating derivatives from the tail to the head of the model based on the chain rule, which is called back propagation [26]. Conversely, calculating output or loss function of a model when given an input is called forward propagation.

As training progresses, most of the loss values in a minibatch become very small. However, there are still some examples where the loss values are relatively large. We can find analogs of these in the test results. When we conduct vehicle detection with a trained classifier, many of the bounding boxes are classified correctly, but still there can be some that are misclassified. These are sometimes called hard examples. For instance, they may have vehicle-like features that are difficult to discriminate (see Figure 6 for examples).

Figure 6. Instances of hard example patches.

Such examples are likely to give clues to discriminating confusing features; therefore, utilizing them in training processes seems to yield better accuracy. However, they would not sufficiently contribute to learning in an ordinary SGD. As described above, most loss values in a minibatch become very small as training progresses, and gradients calculated over a minibatch are aggregated and averaged. This means the few informative examples are diluted by another large part of the minibatch that do not contribute to improving accuracy. In this way, hard examples contribute little to learning. To address this, we needed to choose the informative examples and preferentially use them for training, which is called hard example mining.

2.2. Hard Example Mining (HEM) in SGD Training

In HEM, hard examples, which are difficult to classify correctly, are weighted more than other examples for training. Typically, hard examples are selected if they are difficult to correctly classify for a current classifier. HEM has been conventionally used in machine learning, e.g., for SVM training. For pedestrian detection, Dalal and Triggs [13] searched hard examples with a preliminarily trained detector and additionally used them for training a final detector. Felzenszwalb et al. [27] iteratively updated the training data subset by discarding easy examples that were correctly classified beyond the current classifier's margin and adding hard examples that violated the current classifier's margin. Using a non-SVM method, Tang et al. [16] adopted a cascade of boosted classifiers of shallow decision trees as the final classification part of their vehicle detection method. In each stage of their Real AdaBoost [21] training, a weak classifier that best classified the training data was selected as part of the final classifier. The misclassified examples were weighted, and the candidate weak classifiers in the next stage were imposed on well classifying those weighted hard examples.

In object detection by deep learning, a heuristic method has been previously used. In Fast R-CNN [7] and SPP-net [8], when sampling reference background patches for training data, if the IoU between a background patch and a foreground patch is lower than 0.1, the sampled background patch is excluded from training data, because the patch is not a hard example given that the patch is easily classified to the background patch. If a background patch overlaps a foreground patch in a much portion, such as cases where the IoU is much higher than 0.1, the patch is chosen as training data because the patch is useful as a hard example as the background patch is likely to be confused with the foreground. This improves accuracy to some extent but is suboptimal, as there could be some hard examples in the excluded patches.

To address this, Shrivastava et al. [22] proposed Online Hard Example Mining (OHEM). In OHEM, the loss values of all region proposals in an image are calculated by the current classifier and only examples with the largest losses are picked for a minibatch. OHEM further improved accuracy over the heuristic method.

However, we could not directly apply OHEM to our method because OHEM is designed for Fast R-CNN, a training process that is different from ours. In Fast R-CNN training, an image is randomly selected from all training images, region proposals are calculated in the image, and 64 of them are selected for a minibatch (in practice, their minibatch consists of 128 examples from two images). As Fast R-CNN employs RoI pooling—in which the feature map is calculated from an entire image only once and region proposals are classified by projecting each of them onto the feature map—this image-wise training is effective. OHEM replaces the selection of region proposals for a minibatch and also benefits from RoI pooling in terms of effective computation. Meanwhile, in our algorithm proposed in Section 2.1.1., we preliminarily extracted patches from all training images, and sampled minibatches randomly from them. We needed to modify OHEM to our training procedure.

Here we explain our method in detail. Figure 7 shows an overview of the algorithm.

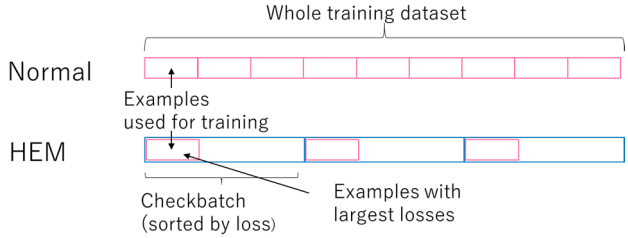

Figure 7. Algorithm overview. Loss values are calculated in each checkbatch and only examples with the largest losses are used for training.

First, we shuffled the entire training dataset and partitioned it into batches of size *ncheck*. We called each batch a checkbatch, and *ncheck* is the number of examples where the loss values are checked in one iteration. Then, we processed each checkbatch one by one. In each checkbatch, we calculated the loss values with a current classifier, sorted examples by loss values in descending order, picked *nlearn* examples with the largest losses, and used them for training to update the current classifier; *nlearn* is the number of examples that are actually used for training. This process was repeated over epochs until convergence. While *ncheck* was larger than *nlearn*, the ratio can be decided arbitrarily. The algorithm is summarized in Algorithm 1.

Algorithm 1: Hard example mining in SGD

Input: Training dataset D, *nlearn*, *ncheck*, *epochs*, classifier f
Output: Trained classifier f
Initialize variables of f
For e = 1 to *epochs*:
    Shuffle D
    Split D into size(D)/*ncheck* checkbatches
    For each checkbatch:
        Compute loss values of examples in the checkbatch by f
        Sort the examples in the checkbatch by loss values in descending order
        Train f using the top *nlearn* examples

In this way, for training, only the examples with the largest losses are always used, which are the most informative ones. We expect our method to promote the learning of finer features, and it should also find the optimal balance of positive and negative examples in the training examples, the same as in [22]. Recall that SGD is based on the assumption that each minibatch approximates the entire training dataset well, as described in Section 2.1.2. From this viewpoint, we can say that our proposed method approximates checking the loss values of all the training data and only selected the most informative examples for training in one iteration.

In plain SGD, the entire training dataset is split into minibatches and each minibatch is used for training, which means all the examples in the training data are used for training. However, in the proposed method, we only used a part of the examples for training in one epoch because we selected only the examples with the largest loss values. Therefore, we compared plain SGD and the proposed method in the same iteration, not in the same literal epoch.

Here, we also explain the implementation details. As is common practice, we adopted softmax cross entropy as the loss function as defined as follows:

$$\mathrm{loss}(y, t) = -\frac{1}{N}\sum_{n=1}^{N}\sum_{c=1}^{C} t_{nc}\, ln\, y_{nc}, \tag{4}$$

where y is the softmax output; N is minibatch size; C is the number of classes; and t is a label. Only one true label among C is 1 and the others are 0. According to this equation, when we want to sort examples of a minibatch by loss values, we only need to check the prediction results, i.e., the last activation of the model corresponding to the true class.

There are two ways to implement the proposed method. The first is to calculate all of the loss values in a checkbatch, set the loss values to zeros (except the largest ones), and train. The second is to preliminarily select examples with the worst prediction results in a checkbatch, calculate their loss values, and train. We adopted the second procedure in this paper, mainly because we introduced batch normalization layers [23] into our CNN, as mentioned in Section 2.1.1. Batch normalization normalizes a minibatch so that the mean and the variance of the minibatch become 0 and 1, respectively. If the first implementation is adopted, after examples with the largest losses in a checkbatch are selected, the batch normalization needs to be re-calculated, because the minibatch statistics are generally changed. However, we cannot recalculate the batch normalization by linear transformation of the previous forward propagation result because our CNN also has non-linear ReLU layers as mentioned in Section 2.1.1. Therefore, there is a need to recalculate the loss values of the selected examples after all. For this reason, we adopted the second implementation.

Batch normalization has a training mode and a testing mode, and different statistics are used to normalize a minibatch in each mode. In the training mode, it uses the statistics of the current minibatch, and in testing mode it uses the statistics of all the data that have been used for training. We used the testing mode in the loss checking process, because our idea was to use examples that were difficult to classify by the current classifier.

2.3. Accuracy Assesment

2.3.1. Vehicle Detection Criteria

We adopted the same criteria as [12]. When a window was detected as containing vehicles, if the distance of centers between it and any groundtruth was smaller than 0.45 of the window size, it was judged as true positive (TP), otherwise it was a false positive (FP). A groundtruth was judged to be detected if it had at least one corresponding TP. In these criteria, it is possible to have multiple TPs for one vehicle, which are redundant except for one TP. One TP is allowed to detect only one vehicle.

2.3.2. Quantitative Measure

We calculated the recall rate (RR), precision rate (PR), and false alarm rate (FAR) as per [12,14]. We also calculated the F1 scores by using the obtained RR and PR scores.

$$\mathrm{RR} = \frac{\text{detected groundtruths}}{\text{groundtruths}}$$

$$\mathrm{PR} = \frac{\text{detected groundtruths}}{\text{detected windows}}$$

$$\mathrm{FAR} = \frac{\text{false positives}}{\text{groundtruths}}$$

$$\mathrm{F1} = \frac{2 \times \mathrm{PR} \times \mathrm{RR}}{\mathrm{PR} + \mathrm{RR}}$$

3. Experiment and Results

We evaluated the performance of our method by comparing it with plain SGD training (hereinafter called the normal method). First, we trained CNNs by the normal and proposed methods, and then conducted vehicle detection with those classifiers. An overview of the experiment is shown in Figure 8.

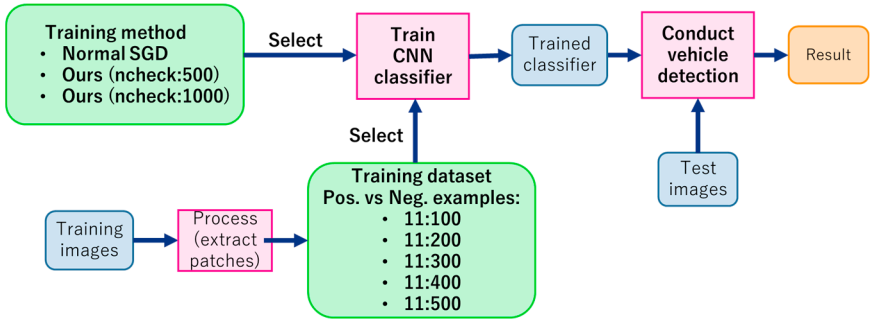

Figure 8. Experiment overview.

We used sparse training data as explained in Sections 3.1 and 3.2. We conducted preliminary experiments using the normal method and found that it still had room for improvement, because the FAR in the result was high. We aimed to reduce false positives and improve the accuracy by using the proposed method, which was the first motivation of this paper.

3.1. Training and Test Images

We downloaded aerial ortho images of New York from the U.S. Geological Survey (USGS), cut out areas of harbors and malls, and used them for training and testing. The pixel size of all images was 0.15 m. Table 1 shows the images and their attributes. The train_2 image was taken in the spring of 2013, and the rest was taken in April–May of 2014. These were the only images used in this paper.

Table 1. Training and test images.

	Training Images		Test Images	
	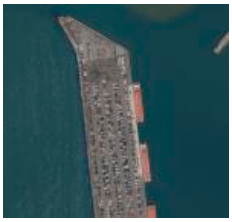		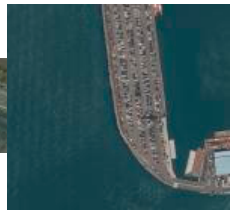	
Name	train_1	train_2	test_1	test_2
City	New York		New York	
Feature	Harbor	Mall	Harbor	Mall
Area	0.16 km^2	0.08 km^2	0.16 km^2	0.12 km^2
Vehicle	687	821	806	510

3.2. Data Preparation

We prepared groundtruth maps of all the images described in Section 3.1 by choosing a pixel in the center of each vehicle by hand. Then we generated the training dataset by extracting patches from the training images. For positive examples, we first extracted bounding boxes around the dots in the groundtruth maps as groundtruth patches. The window size was 50 pixels, which was designed to well cover the typical size of vehicles. To increase the variance of the positive examples, we generated 10 rotated duplications of each groundtruth patch at rotation angles from 9° to 90° in increments of 9°. This is called data augmentation. Then, for negative examples, we extracted background patches randomly where the IoU between a candidate patch and any groundtruth was lower than 0.4. These types of methods are commonly used. The authors in [14] used similar methods for data preparation. Finally, all patches were resized to 48 by 48 pixels, which was the input size of our CNN.

We generated five different training datasets. The groundtruth patches were always the same, whereas the amounts of sampled background patches were different. The ratios of background patches to groundtruth patches (without the augmented ones) were 100:1, 200:1, 300:1, 400:1, and 500:1 (hereinafter called $\times$100, $\times$200, $\times$300, $\times$400, and $\times$500), respectively. For instance, in the case of $\times$100, the ratio of positive examples (including augmented ones) to negative examples was 11:100. We used them, because the balance of positive and negative examples in the training data generally affects the result, and we aimed to evaluate this effect. As the background area is generally larger than the foreground area in an image, it is common to use more negative examples than positive examples in the training data for better accuracy [1,7,8,11,14]. This is more conspicuous in the case of vehicle detection, because vehicles are small objects. Taking these into account, we began the ratio of positive to negative examples from 11:100.

In each training dataset, we randomly selected one-tenth of the dataset and used it as a fixed hold-out validation dataset. During training, we calculated the loss and accuracy on this validation dataset in every epoch, which was its only use.

3.3. Experiment

We trained classifiers with the normal method and our proposed method. In the proposed method, we used two *ncheck* values of 500 and 1000 (hereinafter called HEM500 and HEM1000, respectively) to evaluate the effect of this parameter. Due to our limited computing resources, we could test only these cases. For each training method, we used the $\times$100, $\times$200, $\times$300, $\times$400, and $\times$500 datasets as described in Section 3.2. After training, we conducted vehicle detection tests with these trained classifiers. Table 2 shows all the experimental conditions, which are combinations of the training method and the background patch amount.

Table 2. Experimental conditions, which are combinations of the training method and the background patch amount. Each pair in parentheses expresses one experimental condition.

		Training Method		
		Normal	**HEM500**	**HEM1000**
BG patch amount	×100	(×100, Normal)	(×100, HEM500)	(×100, HEM1000)
	×200	(×200, Normal)	(×200, HEM500)	(×200, HEM1000)
	×300	(×300, Normal)	(×300, HEM500)	(×300, HEM1000)
	×400	(×400, Normal)	(×400, HEM500)	(×400, HEM1000)
	×500	(×500, Normal)	(×500, HEM500)	(×500, HEM1000)

Since we trained the CNN classifiers from scratch and initialized the weight variables randomly, the performances of the trained classifiers were slightly different. To mitigate these fluctuations, we repeated all experiments under each condition 10 times and averaged the results. The standard deviations and standard errors are shown in the result tables.

3.4. Training Results

We initialized the CNN weight variables at random. We used the Adam solver [28], and the training iterations were equivalent to 100 epochs in the normal method. (e.g., 500 epochs when *ncheck* was five times larger than *nlearn*). The batch size for learning (i.e., *nlearn*) was constantly 100. These were decided empirically based on preliminary experiments. In every epoch during training, the mean loss and mean accuracy were calculated for the training and validation datasets.

As the shapes of all of the graphs were similar for the different conditions, we present only one example. Figure 9 shows the training curves where the background patch amount was ×200 (one of the results of repeated experiments). In Figure 9, all methods seem to have sufficiently converged. For training loss and accuracy, the fluctuations of the proposed method were larger than the normal method. This seems natural because in every iteration, the CNN is updated and used to calculate loss values and select training examples, which means that the criteria of selecting training examples changed in every iteration. Figure 10 shows the moving average of Figure 9d, which aimed to show the convergence trend more clearly. In Figure 10, we averaged about 6350 iterations, which corresponded to two epochs of the normal method.

As Figure 10 shows, while the accuracy in the normal method still improved slightly toward the last epochs, it improved much faster in the proposed method. This means that the proposed method markedly accelerated convergence. In addition, the curve of HEM1000 seems to have converged slightly earlier than that of HEM500. This indicates that the larger *ncheck* accelerated convergence more.

To evaluate the training results, we compared the final values of validation loss and validation accuracy under different conditions. To mitigate fluctuations, we calculated the moving average of iterations corresponding to 10 epochs of the normal method and then averaged the repeated experiments. Table 3 shows the statistics, which include the standard deviations and standard errors. While validation losses were not necessarily smaller in the proposed method than in the normal method, validation accuracies were always higher in the proposed method than in the normal method, which can be said explicitly according to the standard errors. Although the main purpose of this validation was to check the overfitting occurrence, this result is evidence that the proposed method yielded better generalization. When we compared the validation accuracies of HEM500 and HEM1000, we could not see a significant difference. Note that this accuracy calculation included classifying the background patches. The performance of our system in terms of vehicle detection is evaluated in Section 3.5.

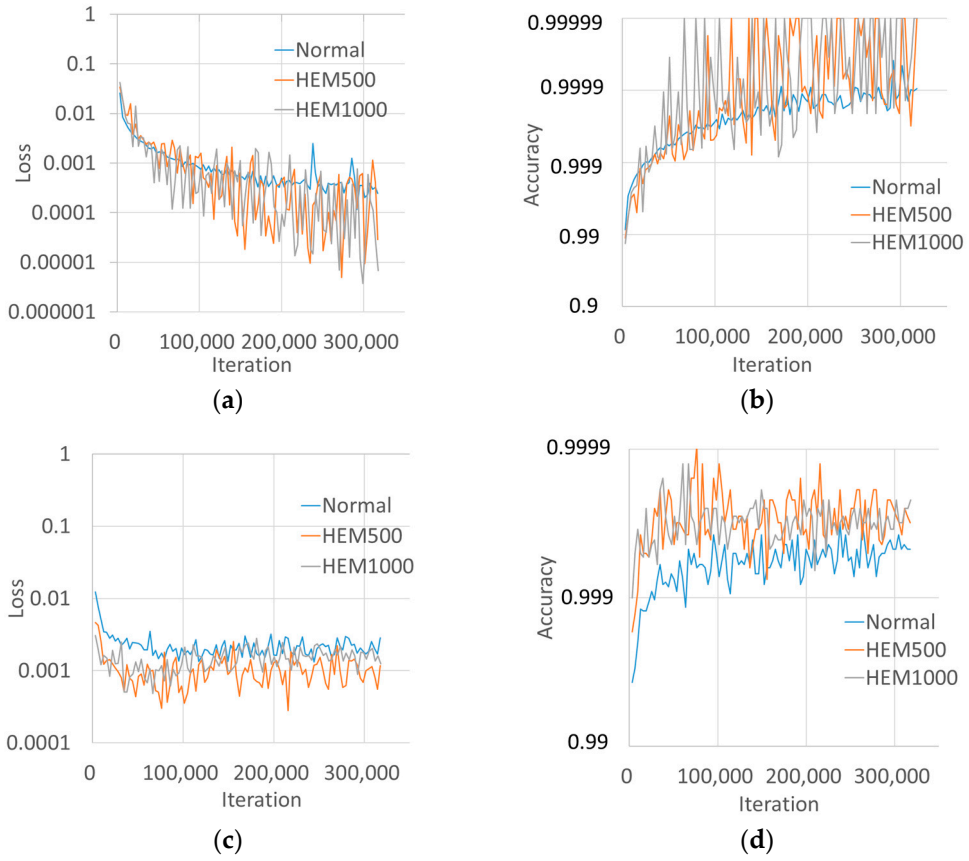

Figure 9. Training curve example. The background patch amount was ×200 in this case. (**a**) Training loss; (**b**) training Accuracy; (**c**) validation loss; and (**d**) validation accuracy.

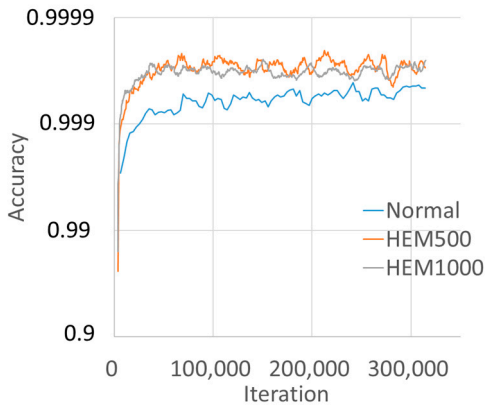

Figure 10. Moving average of Figure 9d.

Table 3. Statistics of the last values of validation loss and validation accuracy. We calculated the moving average graphs and averaged the repeated experiments. Here we emphasized the best accuracy among methods in bold font.

BG Patch	Training Method	Last Validation Loss			Last Validation Accuracy		
		Average	STDDEV	STDERR	Average	STDDEV	STDERR
×100	Normal	0.0031	0.0006	0.0002	99.932%	0.013%	0.004%
	HEM500	**0.0030**	0.0005	0.0002	**99.950%**	0.005%	0.002%
	HEM1000	0.0036	0.0008	0.0003	99.949%	0.014%	0.005%
×200	Normal	0.0016	0.0004	0.0001	99.957%	0.008%	0.003%
	HEM500	0.0015	0.0005	0.0002	**99.973%**	0.006%	0.002%
	HEM1000	**0.0013**	0.0002	0.0001	**99.973%**	0.002%	0.001%
×300	Normal	**0.0019**	0.0003	0.0001	99.963%	0.007%	0.002%
	HEM500	0.0022	0.0005	0.0002	**99.974%**	0.006%	0.002%
	HEM1000	0.0022	0.0004	0.0001	99.973%	0.003%	0.001%
×400	Normal	**0.0016**	0.0003	0.0001	99.969%	0.004%	0.001%
	HEM500	0.0017	0.0002	0.0001	99.978%	0.003%	0.001%
	HEM1000	**0.0016**	0.0003	0.0001	**99.981%**	0.003%	0.001%
×500	Normal	0.0011	0.0002	0.0001	99.978%	0.003%	0.001%
	HEM500	**0.0010**	0.0002	0.0001	**99.986%**	0.003%	0.001%
	HEM1000	0.0011	0.0002	0.0001	**99.986%**	0.002%	0.001%

3.5. Vehicle Detection Results

We conducted vehicle detection using the method described in Section 2.1.1 and the test images described in Section 3.1. Results of repeated experiments were averaged.

Figure 11 shows the F1-measure results and Table 4 shows the statistics of all quantitative measures, which include the standard deviations and standard errors.

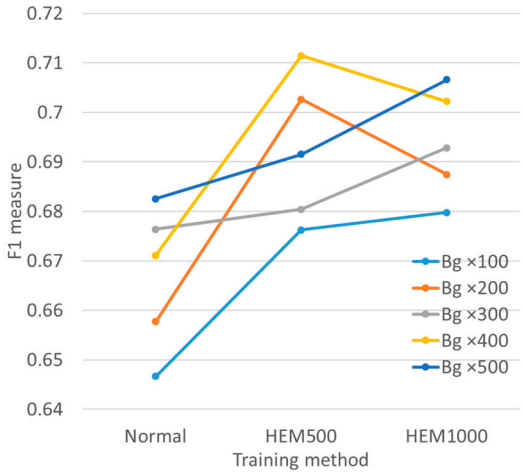

Figure 11. F1 scores in each condition. Our proposed method improved the scores in all cases over the normal method.

In terms of F1 scores, while almost all of the standard errors were smaller than 0.01, the proposed method improved the scores by over 0.02 when compared to the normal method in most cases, which proved the effectiveness of our proposed method. Moreover, because the standard deviations of all methods were not very different, we can say our proposed method worked stably.

Table 4. Statistics of all quantitative measures. Here we emphasized the best accuracy among methods in bold font.

BG Patch	Training Method	FAR			PR			RR			F1		
		Avr.	STDDEV	STDERR	Avr.	STDDEV	STDERR	Avr.	STDDEV	STDERR	Avr.	STDDEV	STDERR
×100	Normal	0.584	0.109	0.036	0.511	0.041	0.014	**0.887**	0.033	0.011	0.647	0.028	0.009
	HEM500	0.481	0.104	0.035	0.554	0.042	0.014	0.873	0.027	0.009	0.676	0.028	0.009
	HEM1000	**0.480**	0.099	0.033	**0.556**	0.042	0.014	0.877	0.012	0.004	**0.680**	0.030	0.010
×200	Normal	0.526	0.073	0.024	0.527	0.031	0.010	**0.879**	0.030	0.010	0.658	0.019	0.006
	HEM500	**0.388**	0.056	0.019	**0.590**	0.027	0.009	0.870	0.017	0.006	**0.703**	0.016	0.005
	HEM1000	0.434	0.066	0.022	0.573	0.031	0.010	0.861	0.017	0.006	0.687	0.020	0.007
×300	Normal	0.452	0.091	0.030	0.555	0.031	0.010	**0.868**	0.014	0.005	0.676	0.021	0.007
	HEM500	0.435	0.071	0.024	0.566	0.038	0.013	0.857	0.029	0.010	0.680	0.021	0.007
	HEM1000	**0.396**	0.066	0.022	**0.587**	0.041	0.014	0.849	0.022	0.007	**0.693**	0.027	0.009
×400	Normal	0.490	0.127	0.042	0.547	0.050	0.017	**0.873**	0.018	0.006	0.671	0.036	0.012
	HEM500	**0.340**	0.081	0.027	**0.616**	0.049	0.016	0.847	0.027	0.009	**0.711**	0.024	0.008
	HEM1000	0.383	0.062	0.021	0.593	0.032	0.011	0.862	0.020	0.007	0.702	0.021	0.007
×500	Normal	0.446	0.063	0.021	0.566	0.030	0.010	**0.861**	0.025	0.008	0.683	0.024	0.008
	HEM500	0.394	0.094	0.031	0.591	0.047	0.016	0.837	0.023	0.008	0.692	0.030	0.010
	HEM1000	**0.370**	0.050	0.017	**0.601**	0.024	0.008	0.858	0.013	0.004	**0.707**	0.016	0.005

When we compared the results in terms of the background patch amount, the F1 scores in the normal method tended to be higher when the background patch amount was larger, and this seems to also apply in the proposed method.

When we compared the F1 scores of HEM500 and HEM1000, from $\times 100$ to $\times 500$, HEM500 won in two cases and HEM1000 won in the other three cases, which seems almost even. The score differences were less than those between the normal method and the proposed method.

Figure 12 plots the FAR versus the RR. As can be seen, the proposed method greatly reduced the FAR while retaining nearly the same RR. This mainly contributed to accuracy improvement, because our training data were sparse and the FARs were relatively large throughout our experiments. Note that the power of the proposed method was not restricted to FAR reduction, because the most informative examples were automatically selected in every checkbatch.

Although the non-maximum-suppression (NMS) was properly applied, there were some duplicated detections (redundant TPs) due to a limitation of NMS. However, this does not affect accuracy assessment according to the definitions of PR and F1.

Figure 13 shows an example of good and bad results by HEM500 where the background patch amount was $\times 400$. We chose the classifiers that achieved the best F1 scores from repeated experiments. While many FPs were reduced in the pair of images in Figure 13a, a few vehicles became undetected in Figure 13b. There seems to have been a kind of trade-off, while overall accuracy was improved.

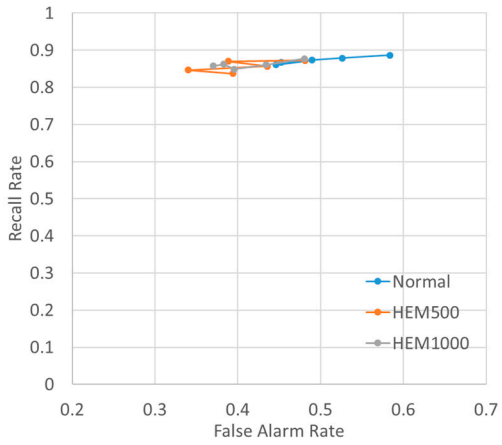

Figure 12. FAR versus RR. Our method greatly reduced the FAR while keeping nearly the same RR.

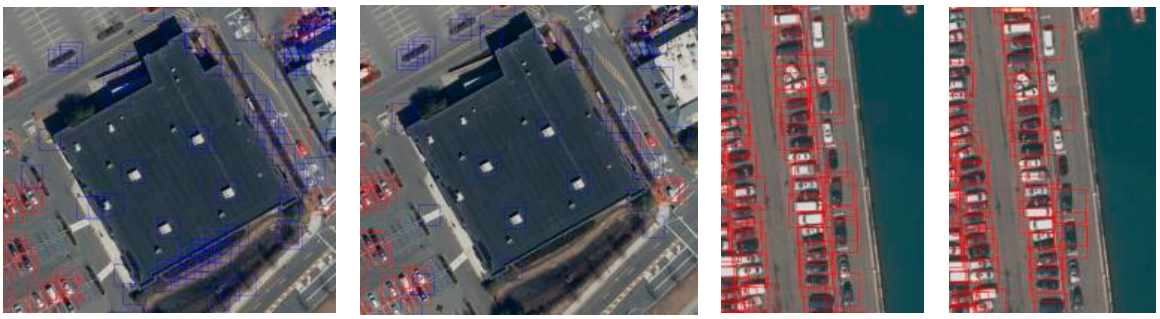

(**a**) (**b**)

Figure 13. An example of good and bad cases in the tested images. In each pair of images, the left one shows the result of the normal method and the right one shows the result of HEM500. (**a**) Good case. On the right, FPs were much reduced; (**b**) bad case. On the right, some vehicles became undetected.

4. Discussion

4.1. Improvement Extent

While we could see that our method improved accuracy, the improvement of F1 did not seem very significant. We investigated the reasons. First, the improvement was different between test_1 image and test_2 image. Table 5 shows the F1 result of each test image in the case of ×400.

Table 5. Average F1 score and improvement of each test image in the case of ×400.

Image	Method		Improvement
	Normal	HEM500	
test_1	0.83	0.82	−0.01
test_2	0.54	0.61	0.07
Both	0.67	0.71	0.04

As can be seen, although the result of test_2 image was much improved, the result of test_1 was originally good, because test_1 image had very similar features to the train_1 image and did not much improve (became slightly worse in this case) using our method. Thus, the improvement of both test images became relatively small.

The second reason was redundant TP. While our method greatly reduced FPs, the improvement of PR was relatively small. In Table 4, in the case of ×400, while FAR reduction was about 0.13 on average, PR improvement was about 0.06 on average. This was because not only FPs, but also redundant TPs hurt PR. As we checked, the ratios of redundant TPs to detected vehicles in normal, HEM500, and HEM1000 were about 0.31, 0.25, and 0.27, respectively. Our method also seems to have reduced redundant TPs, which were because redundant TPs were relatively distant from the vehicles. For example, in one experiment using the normal method with ×400, the average distances between vehicles and TPs that detected vehicles, and between vehicles and redundant TPs, were 6.6 pixels and 11.5 pixels, respectively. As our training data only included positive examples that exactly matched the locations of vehicles, such redundant TPs would have been reduced by HEM. However, the reduction was smaller than that of FPs, because the redundant TPs overlap vehicles to some extent. This diluted the improvement of FAR.

The third reason was RR decrease. In Table 4, in the case of ×400, RR decreased by 0.02 on average. As above-mentioned, our HEM method seems to have reduced TPs that were relatively distant from vehicles, and a small part of them may have detected vehicles before applying HEM. This slightly hurt the RR.

The second and third reasons came from the inaccuracy of sliding windows. By replacing sliding windows with a more accurate method such as RPN, we can see the improvement by HEM more explicitly.

The best average F1 score throughout our experiments was 0.71, which is actually not a state-of-the-art result. For instance, [16] reported an F1 of 0.83, and [18] reported very high F1 of 0.94. Although it is not a fair comparison, because the training data and test settings are totally different, 0.71 is not the best. The primary reason would be the insufficiency of our training data. The authors in [16] used the Munich dataset [29], which has 9433 annotated vehicles, and [18] proposed and used the COWC dataset, which has 32,716 annotated vehicles. Compared to those datasets, our training data were sparse. Although our HEM could improve accuracy, sufficient training data were necessary for high performance. Another reason would be the simplicity of our CNN architecture. When we compared just the numbers of convolutional layers in each method, [16] had five and [18] had 50, whereas our model only had three.

We can combine our HEM method with adequate training data and rich CNN architecture for higher accuracy. Moreover, as discussed above, the accuracy would further become better by improving or replacing the sliding window method. Our HEM method can easily scale with those options.

4.2. Training Loss Values and Duration

Shrivastava et al. [22] reported that the loss values during training became smaller by using their OHEM method because they conducted a fair comparison where all region proposals in an image—not just the ones selected for a minibatch—were used to calculate the loss values in every method. Meanwhile, the loss values of our method seemed to have been better than the normal method; however, the difference was very small (Figure 9a). This was because those loss values were calculated from examples that were actually used for training; those examples had relatively large loss values, because we chose such examples for training. If we evaluated the loss values over a checkbatch, the trend would be similar to [22].

Our method took more time to train for the same iterations than the normal method, because of the overhead of calculating loss values in a checkbatch. For instance, training durations of normal, HEM500, and HEM1000 were 2.5, 6, and 10 h, respectively, with Tesla K20X manufactured by NVIDIA (Santa Clara, CA, USA) in Figure 9. In the original OHEM, it took approximately 1.7 times longer in one iteration to select 64 out of around 4000 region proposals in an image. Our method is more time-consuming than theirs, because our method requires extra forward propagation calculations as described in Section 2.2, whereas the original OHEM can calculate the loss values of region proposals with small additional costs due to RoI pooling.

However, our method strongly accelerates convergence. Therefore, the training could be stopped much earlier in the proposed method, which would cancel out the demerit.

4.3. Source of Accuracy Improvement

In our experiment, more background patches tended to yield better F1 scores in the normal method. This may be because more background patches contain more "negative" features to be discriminated from vehicles, and it kept improving the accuracy in the range of our experiments. FP reduction seems to have contributed more to the performance improvement, because the FAR was relatively high in our experiments.

To confirm how accuracy improvement continued, we conducted additional experiments. We gradually increased the amount of background patches to 1000 times the number of groundtruths. Figure 14 shows all the F1 scores of vehicle detection tests by the normal method, including the additional experiments. The standard deviations and standard errors of the additional experiments had values similar to the previous experiments. As can be seen, the accuracy does not seem to have improved after $\times 600$, which indicates the best balance was around $\times 600$. Although the best score was at $\times 800$, which was about 0.7, the difference from $\times 600$ was smaller than the standard errors, and was thus negligible.

When we compared these results with those of the proposed method, four out of 10 scores of the proposed method surpassed the best scores of the normal method, which had the best balance of positive and negative examples in the training data. This fact proves that our method improved accuracy by learning finer features, and not only by balancing positive and negative examples.

Continuing to increase negative examples could lead to a worse result. Even in such cases, our method is expected to find the optimal balance between positive and negative examples during training, which we could not confirm explicitly in our experiments. This will be our future work.

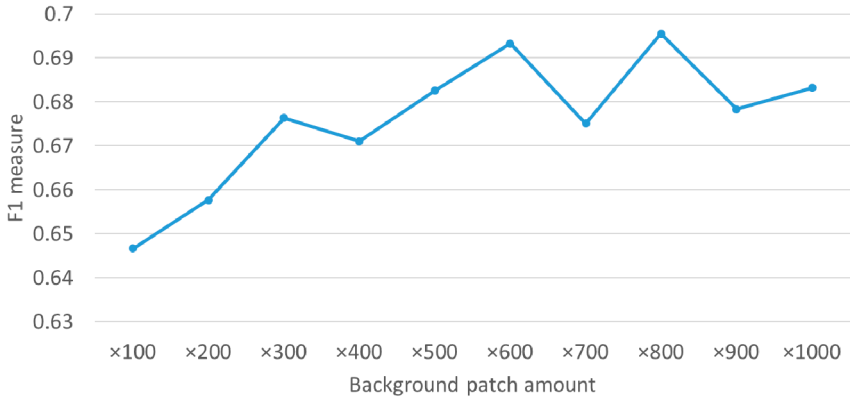

Figure 14. All F1 scores by the normal method including the additional experiments. The score does not seem to have improved after ×600.

4.4. HEM500 vs. HEM1000

The HEM500 and HEM1000 scores were almost even, and the score differences were less than those between the normal and proposed methods. Considering that the validation accuracy results of HEM500 and HEM1000 were not very different, and taking these results into account, we can suppose that the performances of HEM500 and HEM1000 were similar, because an *ncheck* value of 500 was large enough, and increasing it did not improve accuracy in the range of our experiments. However, our experiments were not enough to prove this conjecture. Moreover, we could test only two values of *ncheck* due to our limited computing resources. Further verification will be our future work.

4.5. Usabilty of Our Method

In our experiments, we used a sparse training dataset. However, our method does not depend on model architecture or training data; therefore, it would be effective even when training data are abundant.

In this paper, we used our CNN as a classifier. However, it could also be used as a feature extractor by removing the last fully connected layer, and it could be combined with other classifiers. For instance, Tang et al. [16] used a cascade of boosted classifiers that was fed features extracted by a CNN. We would be able to further improve accuracy by combining our method with such a method.

5. Conclusions

We applied HEM to the SGD training of a CNN vehicle classifier, which successfully promoted learning finer features and improved accuracy. It took more time to train for the same number of iterations; however, this could be canceled out by breaking training earlier, which would be acceptable as the proposed method markedly accelerates convergence. Although we used sparse data in our experiments, our method would be effective even when training data are abundant. However, we could not confirm the effect of balancing positive and negative examples in the training data explicitly, and the effect of checkbatch size was not sufficiently determined. These issues will form the basis of our future work.

Acknowledgments: This study was conducted as part of the Master's program of Yohei Koga, which is supported by the government of Japan. The authors would like to thank Xiaowei Shao and Zhiling Guo for useful discussions.

Author Contributions: Yohei Koga designed the experiment and prepared the manuscript. Hiroyuki Miyazaki and Ryosuke Shibasaki supervised the research and provided conceptual advice. Hiroyuki Miyazaki helped in the revision of the manuscript.

Conflicts of Interest: The authors declare no conflict of interest.

Appendix

In this appendix, we present an example of HEM500 with $\times 400$ to further investigate the result.

Effect of Clutters and Shadows

To evaluate how clutter and shadows impeded vehicle detection, we visualized undetected vehicles. Figure A1 shows 100 out of 211 randomly selected undetected vehicle patches of test_1 and all 31 undetected vehicle patches of test_2.

Figure A1. Visualization of undetected vehicle patches. (**a**) Undetected vehicles in test_1 image; (**b**) undetected vehicles in test_2 image. The red rectangle patch is covered by a shadow.

As can be seen in Figure A1b, only one undetected vehicle was covered by any clutter or shadows. Although we could not fairly evaluate the robustness of the performance of our sliding window method, because our test images did not originally have many obstacles, there seems to have been only a few vehicles that were not detected due to clutter and shadows.

Furthermore, to evaluate how clutter and shadows confused CNN, we visualized the FP patches. Figure A2 shows all 18 FP patches of test_1 and 100 out of 231 randomly selected FP patches of test_2.

In Figure A2b, several patches with shadows were misclassified as vehicles. This was probably because the shadows looked like straight edge features that are similar to vehicle features, thus confusing CNN. This seems to have been caused by the insufficiency of the classification performance of CNN rather than the inaccuracy of the sliding windows. These misclassifications would be further reduced by using abundant training data.

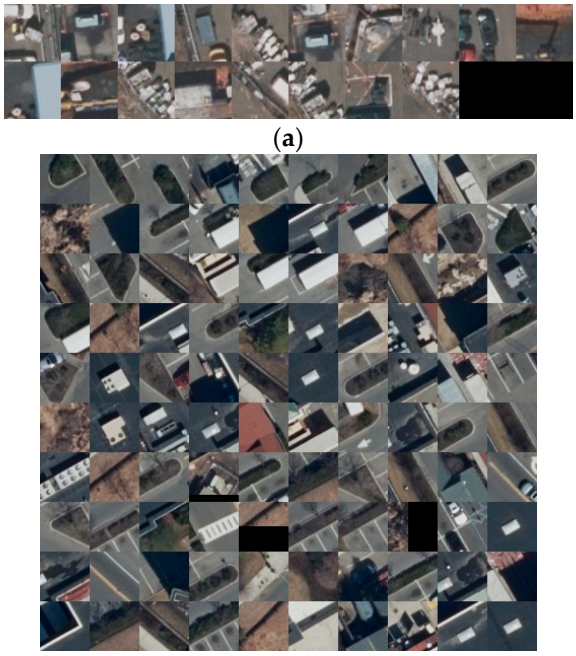

(**a**)

(**b**)

Figure A2. Visualizations of FP patches. (**a**) FP patches in test_1 image; (**b**) FP patches in test_2 image.

References

1. Digital Globe. Available online: https://www.digitalglobe.com/ (accessed on 30 November 2017).
2. Planet Labs. Available online: https://www.planet.com/ (accessed on 30 November 2017).
3. Black Sky. Available online: https://www.blacksky.com/ (accessed on 30 November 2017).
4. NTT Geospace. Available online: http://www.ntt-geospace.co.jp/ (accessed on 30 November 2017).
5. Girshick, R.; Donahue, J.; Darrell, T.; Malik, J. Rich Feature Hierarchies for Accurate Object Detection and Semantic Segmentation. In Proceedings of the 2014 IEEE Conference on Computer Vision and Pattern Recognition (CVPR'14), Columbus, OH, USA, 23–28 June 2014; pp. 580–587.
6. Uijlings, J.R.R.; Sande, K.E.A.v.d.; Gevers, T.; Smeulders, A.W.M. Selective Search for Object Recognition. *Int. J. Comput. Vis.* **2013**, *104*, 154–171. [CrossRef]
7. Girshick, R. Fast R-CNN. In Proceedings of the 2015 IEEE International Conference on Computer Vision (ICCV'15), Santiago, Chile, 7–13 December 2015; pp. 1440–1448.
8. He, K.; Zhang, X.; Ren, S.; Sun, J. Spatial Pyramid Pooling in Deep Convolutional Networks for Visual Recognition. *IEEE Trans. Pattern Anal. Mach. Intell.* **2015**, *37*, 1904–1916. [CrossRef] [PubMed]
9. Ren, S.; He, K.; Girshick, R.; Sun, J. Faster R-CNN: Towards real-time object detection with region proposal networks. In Proceedings of the 28th International Conference on Neural Information Processing Systems (NIPS'15), Montreal, QC, Canada, 7–12 December 2015; pp. 91–99.
10. Redmon, J.; Divvala, S.; Girshick, R.; Farhadi, A. You Only Look Once: Unified, Real-Time Object Detection. In Proceedings of the 2016 IEEE Conference on Computer Vision and Pattern Recognition (CVPR), Las Vegas, NV, USA, 27–30 June 2016. [CrossRef]
11. Liu, W.; Anguelov, D.; Erhan, D.; Szegedy, C.; Reed, S.; Fu, C.Y.; Berg, A.C. SSD: Single Shot MultiBox Detector. In *Lecture Notes in Computer Science, Proceedings of the ECCV 2016: Computer Vision—ECCV 2016, Amsterdam, The Netherlands, 8–16 October 2016*; Springer: Cham, Switzerland, 2016; Volume 9905, pp. 21–37. [CrossRef]
12. Chen, X.; Xiang, S.; Liu, C.L.; Pan, C.H. Vehicle Detection in Satellite Images by Hybrid Deep Convolutional Neural Networks. *IEEE Geosci. Remote Sens. Lett.* **2014**, *11*, 1797–1801. [CrossRef]
13. Dalal, N.; Triggs, B. Histograms of oriented gradients for human detection. In Proceedings of the 2005 IEEE Computer Society Conference on Computer Vision and Pattern Recognition (CVPR'05), San Diego, CA, USA, 20–25 June 2005; Volume 1, pp. 886–893. [CrossRef]

14. Qu, S.; Wang, Y.; Meng, G.; Pan, C. Vehicle Detection in Satellite Images by Incorporating Objectness and Convolutional Neural Network. *J. Ind. Intell. Inf.* **2016**, *4*, 158–162. [CrossRef]
15. Cheng, M.M.; Zhang, Z.; Lin, W.Y.; Torr, P. BING: Binarized Normed Gradients for Objectness Estimation at 300fps. In Proceedings of the 2014 IEEE Conference on Computer Vision and Pattern Recognition(CVPR), Columbus, OH, USA, 23–28 June 2014; pp. 3286–3293. [CrossRef]
16. Tang, T.; Zhou, S.; Deng, Z.; Zou, H.; Lei, L. Vehicle Detection in Aerial Images Based on Region Convolutional Neural Networks and Hard Negative Example Mining. *Sensors* **2017**, *17*, 336. [CrossRef] [PubMed]
17. Car Localization and Counting with Overhead Imagery, an Interactive Exploration. Available online: https://medium.com/the-downlinq/car-localization-and-counting-with-overhead-imagery-an-interactive-exploration-9d5a029a596b (accessed on 27 July 2017).
18. Mundhenk, T.N.; Konjevod, G.; Sakla, W.A.; Boakye, K. A Large Contextual Dataset for Classification, Detection and Counting of Cars with Deep Learning. In *Lecture Notes in Computer Science, Proceedings of the ECCV 2016: Computer Vision—ECCV 2016, Amsterdam, The Netherlands, 8–16 October 2016*; Springer: Cham, Switzerland, 2016; Volume 9907, pp. 785–800.
19. Szegedy, C.; Liu, W.; Jia, Y.; Sermanet, P.; Reed, S.; Anguelov, D.; Erhan, D.; Vanhoucke, V.; Rabinovich, A. Going deeper with convolutions. In Proceedings of the 2015 IEEE Conference on Computer Vision and Pattern Recognition (CVPR), Boston, MA, USA, 7–12 June 2015; pp. 1–9. [CrossRef]
20. He, K.; Zhang, X.; Ren, S.; Sun, J. Deep Residual Learning for Image Recognition. In Proceedings of the 2016 IEEE Conference on Computer Vision and Pattern Recognition (CVPR), Las Vegas, NV, USA, 27–30 June 2016; pp. 770–778. [CrossRef]
21. Schapire, R.E.; Singer, Y. Improved Boosting Algorithms Using Confidence-rated Predictions. *Mach. Learn.* **1999**, *37*, 297–336. [CrossRef]
22. Shrivastava, A.; Gupta, A.; Girshick, R. Training Region-Based Object Detectors with Online Hard Example Mining. In Proceedings of the 2016 IEEE Conference on Computer Vision and Pattern Recognition (CVPR), Las Vegas, NV, USA, 27–30 June 2016; pp. 761–769. [CrossRef]
23. Ioffe, S.; Szegedy, C. Batch normalization: Accelerating deep network training by reducing internal covariate shift. In Proceedings of the 32nd International Conference on International Conference on Machine Learning (ICML'15), Lille, France, 6–11 July 2015; Volume 37, pp. 448–456.
24. CS231n: Convolutional Neural Networks for Visual Recognition. Available online: http://cs231n.github.io/optimization-1/#gd (accessed on 27 July 2017).
25. UFLDL Tutorial. Available online: http://ufldl.stanford.edu/tutorial/supervised/OptimizationStochasticGradientDescent/ (accessed on 27 July 2017).
26. Neural Networks and Deep Learning (CHAPTER 2). Available online: http://neuralnetworksanddeeplearning.com/chap2.html (accessed on 27 July 2017).
27. Felzenszwalb, P.F.; Girshick, R.B.; McAllester, D.; Ramanan, D. Object Detection with Discriminatively Trained Part-Based Models. *IEEE Trans. Pattern Anal. Mach. Intell.* **2010**, *32*, 1627–1645. [CrossRef] [PubMed]
28. Kingma, D.P.; Ba, J. Adam: A Method for Stochastic Optimization. *arXiv*, 2014.
29. Liu, K.; Mattyus, G. DLR 3k Munich Vehicle Aerial Image Dataset. Available online: http://pba-freesoftware.eoc.dlr.de/3K_VehicleDetection_dataset.zip (accessed on 30 November 2017).